

WAVES OF SPACE CHARGE IN CERENKOV-TYPE MICROWAVE DEVICES

V. M. Pikunov and I. A. Chernyavskii

A numerical investigation of the properties of space charge waves of a microwave Cerenkov-type device has been conducted. Amplification of space charge waves at frequencies lying below the critical frequency of a decelerating system, as well as generation of long-wave radiation near this frequency, has been studied.

INTRODUCTION

Microwave Cerenkov-type devices based on periodic waveguides and waveguides with partial dielectric filling are intensively studied at present both theoretically and experimentally. The physical principles of operation of such devices are based on the Vavilov-Cerenkov effect: radiation of electromagnetic waves during transit of particles through a medium with a speed exceeding the speed of light in this medium.

In many experimental works on generation of superhigh frequency waves by heavy-current electron beams (see, e. g., [1]) it is noted that radiation includes a long-wave component, its spectrum lying near the critical frequency of the decelerating system. The nature of such a long-wave radiation has not yet been studied sufficiently well. Below we discuss one of the possible mechanisms of amplification of dragged fields of the electron flow at frequencies lying below the critical frequency of a decelerating system, and also the generation of long-wave radiation near this frequency, that is, a long-wave Cerenkov instability [2].

It is well known that the spectrum of the Vavilov-Cerenkov radiation in dispersionless medium begins with zero frequency and extends to infinitely large frequencies [3]. The electrodynamic systems of Cerenkov devices loaded by the electron beam can be considered as media with time and space dispersion, one of their peculiarities being the presence of opaque regions of frequencies where propagation of electromagnetic waves is impossible. At the same time in these regions (for example, at frequencies below the critical frequency of the decelerating system), the electron waves transporting flows of both the electromagnetic and the kinetic power can propagate and even undergo amplification [4, 5].

To raise the output power of Cerenkov devices use is made of relativistic electron beams obtained with the help of heavy-current electron accelerators. An important relativistic effect is the excitation of rotational fields of the space charge [6]. These fields, jointly with potential Coulomb fields, form dragged fields (fields of the neighboring zone) of electron bunches, localized near them and moving with their speeds. As a consequence, the excited space charge waves carry not only a kinetic flow of power but also a flow of rotational electromagnetic power. In this case the formulas for the calculation of the parameters of space charge waves based on the consideration for potential dragged fields only and mentioned, for example, in [7], are no longer applicable.

The circumstances mentioned above require a more careful investigation of the properties of space charge waves in relativistic Cerenkov devices. This investigation is carried out for the special case, a device based on a waveguide with partial filling by the dielectric. However the conclusions drawn are also valid for other types of microwave Cerenkov devices.

1. BASIC EQUATIONS AND ASSUMPTIONS

Consider a one-section Cerenkov device (Fig. 1) based on a round waveguide of radius r_w , to the inner surface of which a dielectric liner with inner radius r_e and length l is tightly fitted. The permittivity of the liner is a piecewise continuous function, having a real and an imaginary parts:

$$\epsilon = \epsilon'(r; \omega) - i\epsilon''(r; \omega).$$

We replace the cathode and collector regions of the device by segments of semi-infinite smooth waveguides of radius r_w , and take account of the reflections of electromagnetic waves introduced by these regions with the help of transformation coefficients specified for the entrance ($z = 0$) and exit ($z = L$) cross sections of the device. The electrodynamic system under consideration is loaded by a ring-shaped electron beam with the external r_{be} and the internal r_{bi} radii. The electron flow is focused by an infinitely large longitudinal magnetic field, therefore the electron motion is one-dimensional. We also assume that the electron flow excites axial-symmetric electromagnetic fields of the E -type. We shall restrict ourselves to a linear problem, when variable components $a(r)$ of the quantities under consideration $A = a_0(r) + a(r) \exp\{i\omega t\}$ are much smaller than their constant components $a_0(r)$.

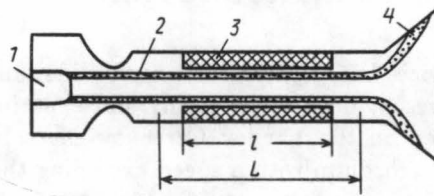


Fig. 1

Schematic diagram of a Cerenkov device based on a waveguide with partial dielectric filling:
(1) cathod; (2) electron beam; (3) dielectric liner; (4) horn.

With regard to the assumptions made above we write down the systems of equations for the determination of variable and constant (in time) quantities:

$$\begin{cases} \text{rot } \mathbf{H} - i\omega \epsilon_0 \epsilon \mathbf{E} = \mathbf{J}, \\ \text{rot } \mathbf{E} + i\omega \mu_0 \mathbf{H} = 0, \\ \frac{dV}{dz} + i\omega V/V_0 = -\eta \overline{E_z}/(\gamma_0^3 V_0), \\ \frac{dJ}{dz} + i\omega \rho = 0, \\ \mathbf{J} = (\rho_0 V + \rho V_0) \Psi(r) \mathbf{z}_0, \end{cases} \quad (1)$$

$$\begin{cases} \text{rot } \mathbf{H}_0 = \mathbf{J}_0, \\ \text{div } \epsilon \text{grad } U = -J_0/(\epsilon_0 V_0), \\ V_0/c = \sqrt{U/[mc^2(1 + U/(mc^2))]}, \\ \mathbf{J}_0 = \rho_0 V_0 \Psi(r) \mathbf{z}_0. \end{cases} \quad (2)$$

Here (r, φ, z) are the cylindrical system of coordinates; $\mathbf{E} = \{E_r, 0, E_z\}$, $\mathbf{H} = \{0, H_\varphi, 0\}$ are the studied components of the electromagnetic fields; ρ_0 , V_0 , and J_0 are constant; and ρ , V , and J are variable components of the space charge density, velocity, and current density of the electron beam, respectively; $\eta = |e|/m$; e and m are the charge and the rest mass of an electron; U is the scalar potential; c is the speed of light; $\gamma_0 = 1 + U/(mc^2)$ is the relativistic Lorentz factor; an upper bar means averaging over the electron beam cross section; $\Psi(r)$ is the given distribution function of the beam current over radius.

The first two equations (1) are the Maxwell equations; the third and the fourth equations are linearized equations of the one-dimensional relativistic motion and of continuity, respectively; the fifth equation is the expression for the linear part of the convection current density. The first equation (2) is the Maxwell equation for the constant component of the magnetic field; the second (the Poisson equation) and the third equations can be used to find the constant components of the scalar potential U and of the electron beam velocity V_0 ; the fourth equation is the expression for the constant component of the convection current density.

Let us look for the solutions of Eqs. (1) and (2) satisfying the following additional conditions.

1. The conditions of radiation and excitation of electron waves at the entrance $z = 0$ and the exit $z = L$ cross sections of the Cerenkov device:

$$\begin{pmatrix} \mathbf{E} \\ \mathbf{H} \\ V \\ J \end{pmatrix}_{z=0,L} = \sum_m A_{\pm m} \begin{pmatrix} \vec{\mathcal{E}} \\ \vec{\mathcal{H}} \\ \mathcal{V} \\ \mathcal{J} \end{pmatrix}_{\pm m} + \sum_m T_{\mp m} \begin{pmatrix} \vec{\mathcal{E}} \\ \vec{\mathcal{H}} \\ \mathcal{V} \\ \mathcal{J} \end{pmatrix}_{\mp m} + \sum_m \begin{pmatrix} \vec{\mathcal{E}} \\ \vec{\mathcal{H}} \\ \mathcal{V} \\ \mathcal{J} \end{pmatrix}_{\pm m} \sum_n T_{\mp m} \Gamma_{\pm m \mp n}, \quad (3)$$

where $(\vec{\mathcal{E}}, \vec{\mathcal{H}}, \mathcal{V}, \mathcal{J})_{\pm m}$ are, respectively, the electromagnetic fields, the velocity, and the current density of proper electron waves in a smooth waveguide loaded by an electron beam, which are propagating in the forward (+) and backward (-) directions; $\Gamma_{\pm m \mp n}$ are the coefficients of transformation of normal electron waves of the smooth waveguide by the inhomogeneities of the entrance and exit routes of the Cerenkov device; $A_{\pm m}$ are the given amplitudes of the electron waves at the entrance and the exit of the device; $T_{\mp m}$ are the unknown amplitudes of electron waves emitted at the entrance and exit cross sections, which are to be determined; $m, n = 1, 2, \dots$

2. The boundary conditions at the discontinuity surface of the dielectric for the tangential component of the electric field

$$E_\tau|_{r=r_{e+0}} = E_\tau|_{r=r_{e-0}}. \quad (4)$$

3. The boundary conditions at the metal surface of the waveguide:

$$E_\tau|_{r=r_w} = 0. \quad (5)$$

4. The conditions of equality of the scalar potential to the accelerating voltage at the surface and its boundedness on the waveguide axis:

$$U_\tau|_{r=r_w} = U_0, \quad U|_{r=0} \leq \text{const}. \quad (6)$$

Equations (1) and (2) combined with boundary conditions (3)–(6) reflect the self-consistent process of interaction of electrons and electromagnetic fields in a linear approximation.

2. ELECTRON WAVES OF THE CERENKOV DEVICE

Let us use the results and notation from [2, 5, 8] and reduce the initial equations and boundary conditions to the boundary-value problem for the homogeneous system of ordinary differential equations

$$\begin{cases} \frac{d\mathbf{W}}{dz} = \hat{F}\mathbf{W}, \\ \hat{D}^{(1)}\mathbf{W}(0) = \mathbf{b}^{(1)}, \\ \hat{D}^{(2)}\mathbf{W}(L) = \mathbf{b}^{(2)}, \\ z \in [0, L]. \end{cases} \quad (7)$$

Here \mathbf{W} is the vector of length $2N + 2$ containing complex amplitudes of the electric $\mathbf{W}^{(e)}$ and magnetic $\mathbf{W}^{(h)}$ fields of waves of the decelerating structure and variable components of the velocity V and of the convective current J (the transposed vector $\mathbf{W}^T = \{\mathbf{W}^{(e)T}, \mathbf{W}^{(h)T}, V, J\}$); \hat{F} is the square matrix of the dimension $(2N + 2)$, depending on the longitudinal coordinate z and describing the interaction of linear waves of the Cerenkov device; $\hat{D}^{(1)}$ and $\hat{D}^{(2)}$ are the rectangular matrices of the boundary conditions of dimensions

$(N + 2) \times (2N + 2)$ and $N \times (2N + 2)$, respectively; $\mathbf{b}^{(1)}$ and $\mathbf{b}^{(2)}$ are the vectors of lengths $N + 2$ and N , respectively, containing the given amplitudes of the fields at the entrance and exit of the device; the vector $\mathbf{b}^{(1)}$ contains in addition the amplitudes of the velocity and the current modulations at the entrance cross section of the device; N is the number of base functions in the Galerkin method. The detailed description of the matrix elements and the structure of the matrices \hat{F} , $\hat{D}^{(1)}$, and $\hat{D}^{(2)}$, and the vectors $\mathbf{b}^{(1)}$ and $\mathbf{b}^{(2)}$ is given in [2, 5, 8]. The boundary-value problem in question for a homogeneous system of ordinary differential equations (7) is among the stiff problems and a special numerical algorithm has been worked out for its solution [8].

The constant components of the electron beam velocity and of the scalar potential can be found by means of the iteration scheme [5].

The decelerating systems of the Cerenkov devices in question contain rather length sections, for which $\hat{F} = \text{const}$ and the problem of electron eigenwaves makes sense:

$$(\hat{F} - \lambda_m \hat{E})\mathbf{e}_m = 0, \quad (8)$$

where λ_m are the eigenvalues of the \hat{F} matrix, which are normalized longitudinal constants of propagation of electron waves $k_z^{(m)} = \lambda_m \omega_0 / V_0$; \mathbf{e}_m is the eigenvector of the \hat{F} matrix; ω_0 is the critical frequency of the waveguide of radius r_w , $m = 1, 2N + 2$. The numerical solution to the complete eigenvalue problem (8) makes it possible to construct the real and imaginary parts of the dispersion characteristic $(\omega/\omega_0, \lambda_m)$.

Moreover, the eigenvector $\mathbf{e}^{(m)}$ determines the structure of the electric $\vec{\mathcal{E}}^{(m)}$ and magnetic $\vec{\mathcal{H}}^{(m)}$ fields, the values of the velocity $\mathcal{V}^{(m)}$ and the current $\mathcal{J}^{(m)}$ components of the electron wave in the chosen point of the dispersion characteristic [5]. For each electron wave the theorem of the kinetic power flow, the Chou theorem, is valid:

$$(1/2)\text{Re} \oint_S [\vec{\mathcal{E}}^{(m)} \times \vec{\mathcal{H}}^{(m)*}] ds = (1/2)\text{Re} \oint_S V_{\text{kin}}^{(m)} \vec{\mathcal{J}}^{(m)*} ds,$$

where $V_{\text{kin}}^{(m)} = \gamma_0^3 V_0 \mathcal{V}^{(m)} / \eta$ is the relativistic kinetic potential of the m th electron wave.

Let us introduce in our consideration fluxes of the kinetic $S_m^{(e)}$ and electromagnetic $S_m^{(EM)}$ energies carried by the m th electron wave. A knowledge of the kinetic and electromagnetic power fluxes makes it possible to introduce the following classification of electron waves [5]: if $|S_m^{(e)}| \gg |S_m^{(EM)}|$, then such electron waves will be called waves of the space charge; in the case when $|S_m^{(e)}| \ll |S_m^{(EM)}|$, the wave corresponds to the waveguide mode; and if $|S_m^{(e)}| \approx |S_m^{(EM)}|$, such a wave corresponds to the guided wave of the space charge and the waveguide mode (in terms of the theory of guided waves [9]). The sign of the kinetic power flux determines the slow ($S_m^{(e)} < 0$) and the fast ($S_m^{(e)} > 0$) waves of the space charge. The sign of the electromagnetic power flux determines the direct ($S_m^{(EM)} > 0$) and the inverse ($S_m^{(EM)} < 0$) waves of the decelerating system.

The classification of electron waves given here will be used below in the discussion of the numerical results.

3. NUMERICAL INVESTIGATION OF SPACE CHARGE WAVES

At first we discuss the properties of space charge waves in a smooth cylindrical waveguide of radius $r_w = 2.5$ cm loaded with a ring-shaped electron beam with $r_{bi} = 1.1$ cm and $r_{be} = 1.3$ cm. At frequencies below the critical frequency of the waveguide there exist only two propagating waves: the slow wave of the space charge (SWSC) and the fast wave of the space charge (FWSC). The presence of an electron beam in the waveguide leads to a certain upward shift of the cut-off frequency of the lower waveguide mode E_{01} . At frequencies above the critical one the branches of the space charge waves always lie to the right of the branch of the propagating waveguide mode E_{01} . Note that electron loading results only in a deformation of the waveguide mode branches; however there are no intersections between them or with any branches of space charge waves at any energies and at a current lower than the critical one for this waveguide.

For convenience of further presentation we shall introduce the quantity $\zeta_m = S_m^{(e)} / S_m^{(EM)}$ which determines the relation between the kinetic power flux and the electromagnetic power flux, carried by the electron wave with the number m . Table 1 summarizes the results of a numerical calculation of the quantity ζ_m for the

Table 1

ω/ω_0	$\mathcal{E} = 50 \text{ keV}$			$\mathcal{E} = 650 \text{ keV}$			$\mathcal{E} = 2.0 \text{ MeV}$		
	SWSC ζ_1	FWSC ζ_2	E_{01} $1/\zeta_3$	SWSC ζ_1	FWSC ζ_2	E_{01} $1/\zeta_3$	SWSC ζ_1	FWSC ζ_2	E_{01} $1/\zeta_3$
0.6	-12	7	—	-5	3		-3	1.2	—
1.8	-25	21	450	-10	4	13	-4	1.3	7
3.0	-42	34	3 200	-15	8	17	-6	1.5	4.2
4.2	-62	51	12 000	-19	11	55	-7.5	1.8	4.1

slow ($m = 1$) and the fast ($m = 2$) waves of space charge and of the quantity $1/\zeta_m$ for the lower waveguide mode ($m = 3$). It is seen from the table that the flux of the electromagnetic energy of the vortex field carried by space charge waves and the kinetic energy flux carried by the waveguide mode, increase with increasing electron velocity. Thus, an increase of the kinetic energy of the electron flux (\mathcal{E}) may remove marked distinctions between the space charge waves and waveguide modes and one must resort to the concept of electron waves. This conclusion is also confirmed by an investigation of the structure of the electromagnetic fields of space charge waves. If at nonrelativistic energies the electromagnetic field of space charge waves is potential and is localized near the electron flux (dashed curves in Fig. 2), then, with increasing electrons energy the content of the vortex component grows, the field diffuses in the radial direction and becomes volumetric and similar to the field of the lower waveguide mode (solid curves in Fig. 2).

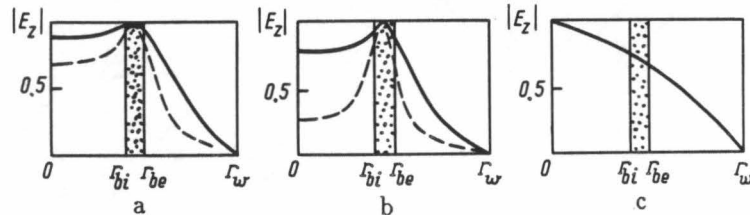


Fig. 2

Transverse distribution of the normalized longitudinal component of the electric field for FWSC (a), SWSC (b) and the E_{01} mode (c) in a smooth waveguide loaded by an electron beam (the dashed line corresponds to $\mathcal{E} = 30 \text{ keV}$, the solid line to $\mathcal{E} = 150 \text{ keV}$).

Consider one-section Cerenkov device on the basis of a round waveguide of the same radius r_w with partial dielectric filling, its dielectric liner having inner radius $r_e = 1.5 \text{ cm}$, $\epsilon' = 3.67$ ($\epsilon'' = 0$), and length $l = 120 \text{ cm}$. The parameters of the electron beam are the direct component of the current I_0 of 0.5 to 6.5 kA and \mathcal{E} of 50 to 650 keV.

The boundary of the Cerenkov instability in energy for an infinite dielectric medium can be estimated according to the formula $\mathcal{E} = 511 [(1 - 1/\epsilon')^{-1/2} - 1] \text{ keV}$, which makes $\mathcal{E} \simeq 88 \text{ keV}$. At a beam energy exceeding this value the Cerenkov instability can arise. However, due to the presence of a gap between the beam and the surface of the dielectric liner (which is typical of the real geometry of the device), the instability region for the lower waveguide mode is displaced far toward the higher frequency region, to which many of the propagating modes correspond. The frequency boundary of the Cerenkov instability depends on the beam energy. As the energy grows, the instability zone shifts down in frequency. For example, at energy $\mathcal{E} = 110 \text{ keV}$ the lower instability zone is situated in the frequency range $\omega/\omega_0 \simeq 3.40$ to 3.90, where four waveguide modes propagate.

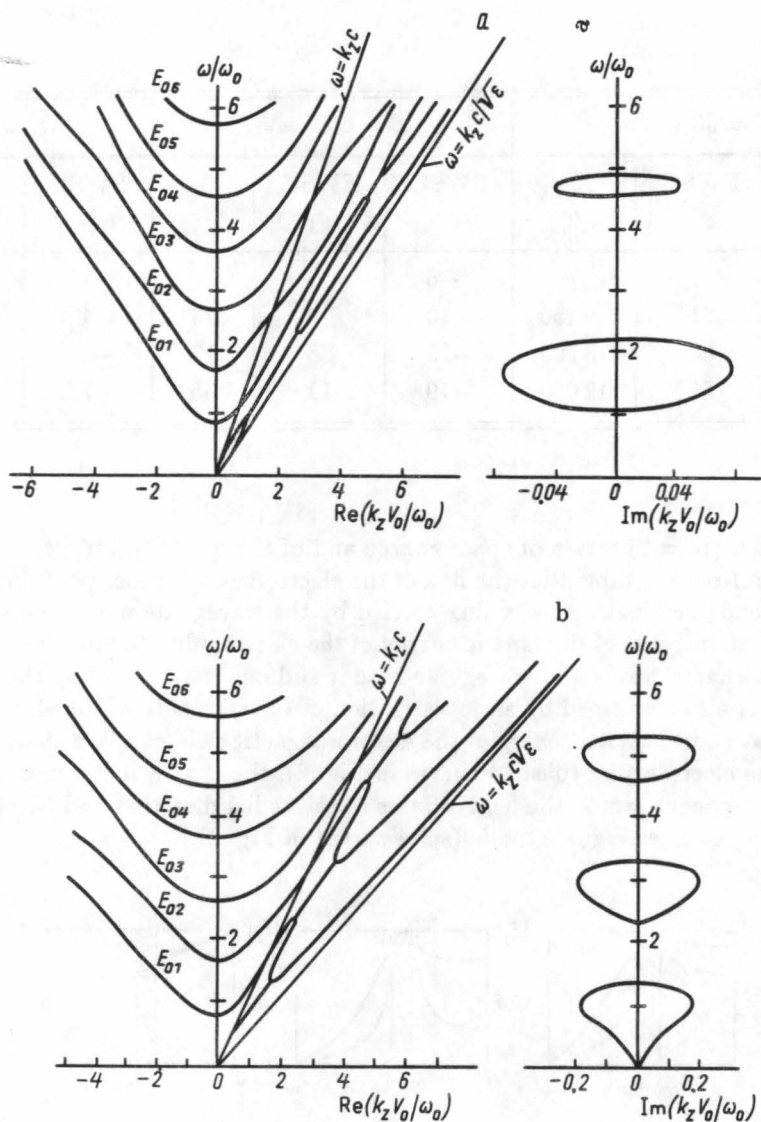


Fig. 3

The real and imaginary parts of the dispersion characteristics of the Cerenkov device at electron kinetic energy \mathcal{E} of 170 keV (a) and 650 keV (b).

Figure 3a shows the dispersion characteristic for the case of $\mathcal{E} = 170$ keV ($I_0 = 1.0$ kA). The lower instability region decreases here to the frequency $\omega/\omega_0 \simeq 1.10$, lying still above the critical one, and it reaches the value of $\omega/\omega_0 \simeq 2.2$. In this frequency range two lower waveguide modes propagate. Table 2 gives the quantity ζ_m at various frequencies for the three branches of the given dispersion characteristic. At frequencies lying beyond the bounds the wave of branch 2 has the property of the waveguide mode ($\zeta_2 \ll 1$), and at $\omega/\omega_0 \simeq 0.7$ the quantity ζ_2 changes its sign, which points to a relation of this wave with SWSC. As branches 1 and 2 approach each other in the frequency range $\omega/\omega_0 \simeq 0.8$ to 1.10, $\zeta_{1,2}$ tends to -1 . Branch 3 in the same range has the properties of the waveguide mode ($\zeta_3 \ll 1$).

Further growth of the beam energy results in the situation when the frequency of the beginning of the lower instability region becomes lower than the cut-off frequency of the waveguide (down to the zero value). Figure 3b shows the dispersion characteristic for the case of $\mathcal{E} = 650$ keV ($I_0 = 6.5$ kA) and Table 2 summarizes the values of ζ_m for the three branches of this dispersion characteristic. At frequencies lying beyond the bounds there are two waves with complex conjugate wave numbers. The real parts of branches 1

Table 2

$\mathcal{E} = 170 \text{ keV}$				$\mathcal{E} = 650 \text{ keV}$			
ω/ω_0	ζ_1	ζ_2	ζ_3	ω/ω_0	ζ_1	ζ_2	ζ_3
0.2	-2.19	0.4	—	0.2	-0.99	-0.99	—
0.6	-2.16	0.08	—	0.5	-0.99	-0.99	—
0.7	-2.10	-0.03	—	0.8	-0.99	-0.99	1.8
0.9	-1.85	-0.33	0.5	1.0	-0.99	-0.99	3.0
1.0	-1.60	-0.55	0.7	1.2	-0.99	-0.99	6.8
1.1	-0.99	-0.99	0.75	1.4	-4.0	-0.16	7.6
1.3	-0.99	-0.99	2.6	1.6	-7.1	-0.03	6.0
1.7	-0.98	-0.98	5.2	1.8	-6.6	-0.01	3.9
2.0	-0.97	-0.97	5.5	2.0	-5.1	-0.004	2.2
2.5	-6.7	-0.06	4.8	2.2	-3.1	-0.002	0.6

and 2 on the dispersion characteristic are merged in a single curve, and the imaginary parts correspond to the growing and to the damped waves. The presence of a region of long-wave instability indicates the interaction of space charge waves.

Upon the appearance of long-wave instability the imaginary parts of the branches on the dispersion characteristic stretch in the direction of low frequencies. In Fig. 3 b the lower region of instability shows a strong stretching and the second region has a weaker stretching. With further growth of the beam energy the same peculiarity appears in higher modes. However, of special interest is the study of the lowest zone of instability, because there are no propagating waveguide modes there.

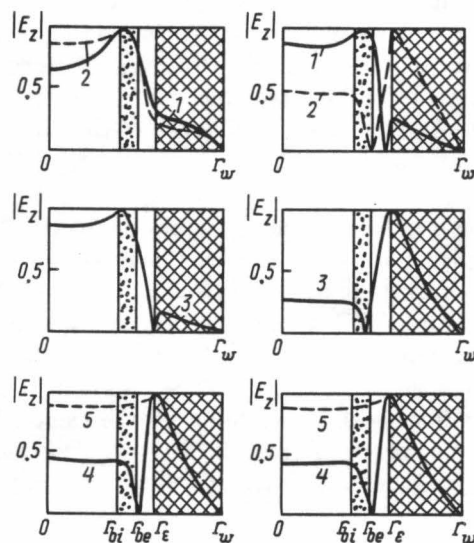


Fig. 4

Transverse distribution of the normalized longitudinal component of the electric field for the first (on the left) and for the second (on the right) branches of electron waves in the Cerenkov device at various energies of the beam at a fixed frequency $\omega/\omega_0 = 0.5$; \mathcal{E} is 70 keV (1), 125 keV (2), 150 keV (3), 197 keV (4), and 650 keV (5).

Table 3

\mathcal{E} , keV	ζ_1	ζ_2	λ , cm
30	-5.5	2.6	—
50	-4.6	1.9	—
70	-4.4	1.7	14.6
100	-3.2	1.0	15.3
125	-3.0	0.9	—
150	-2.5	0.6	37.5
175	-2.0	0.3	52.9
176	-2.0	0.01	—
177	-2.0	-0.01	56.4
185	-1.8	-0.2	77.7
195	-1.3	-0.7	229.3
197	-1.0	-1.0	∞
400	-1.0	-1.0	∞
650	-1.0	-1.0	∞

Let us study the variation of the properties of electron waves as a function of beam energy at a fixed frequency $\omega/\omega_0 = 0.50$ lying below the critical frequency of the dielectric decelerating system. There exist only two branches of propagating electron waves at this frequency. The values of the ratio ζ_m for these waves at various electron energies are given in Table 3. Figure 4 illustrates the variation of the transverse structure of the electron field z -component with growing beam energy. At energies $\mathcal{E} \leq 30$ to 50 keV there exist a fast ($m = 2$) and a slow ($m = 1$) wave of the space charge ($|\zeta_{1,2}| \gg 1$) in the device, which have the transverse field structure similar to the case of a smooth waveguide (see Fig. 2). At $\mathcal{E} \geq 70$ keV branch 2 crosses the line of the light velocity in the dielectric and the field corresponding to this branch penetrates the dielectric (curves 1 in Fig. 4). At $\mathcal{E} \simeq 100$ keV the flux of the vortex electromagnetic field carried by the wave of branch 2 is equal to, and at $\mathcal{E} \simeq 125$ keV is greater than the flux of the kinetic power. This wave starts to show more and more properties of the wave of the decelerating system (Fig. 4, curves 2). At $\mathcal{E} \simeq 150$ keV branch 1 also crosses the line of the light velocity in the dielectric and the field of its wave penetrates the dielectric (Fig. 4, curves 3). With a further increase in energy branches 1 and 2 come closer to each other. At $\mathcal{E} \simeq 177$ keV branch 2 crosses the line $\omega = k_z V_0$ and the respective quantity ζ_2 changes sign: there appears a connection with SWSC. Upon achieving the threshold of the Cerenkov instability for this frequency ($\mathcal{E} = 197$ keV), branches 1 and 2 merge below the line $\omega = k_z V_0$, and the ratio $|\zeta_{1,2}|$ of the power fluxes of the waves becomes of the order of unity. The constants of propagation become complex, and the transverse structure of the fields of both waves becomes the same (Fig. 4, curves 4). Note that both branches in question are among the waves running in the forward direction. With further growth of the flux energy the transverse structure of the field of interacting waves becomes more and more similar to the lower waveguide mode (Fig. 4, curves 5).

The presence of complex roots can lead to amplification of the electron waves in the Cerenkov device at frequencies lying below the critical frequency of the decelerating system. To confirm the conclusion that the electromagnetic radiation in this case can be amplified, a boundary-value problem (7) was solved numerically, when the two propagating electron waves with equal amplitudes were given at the entrance to the device.

At the electron beam energies below the threshold of the Cerenkov instability an oscillatory wave-like process was observed along the device. The picture of the longitudinal distributions of the fluxes $S^{(EM)}$ and $S^{(e)}$ and of the variable component of the current J for the electron energy $\mathcal{E} = 150$ keV and the beam

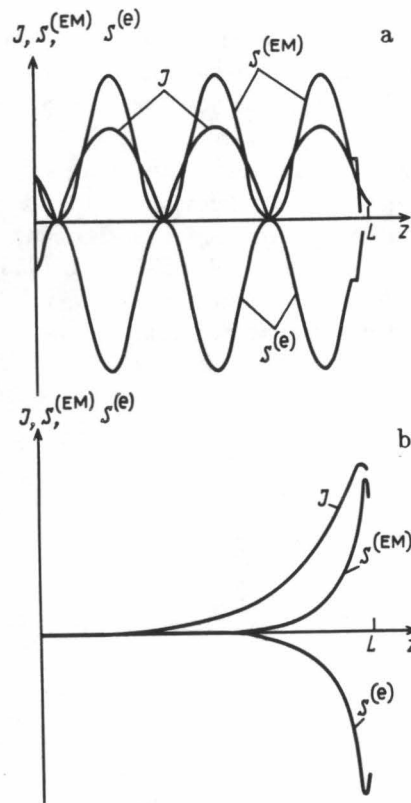


Fig. 5

Distributions of the normalized values of fluxes of the electromagnetic $S^{(EM)}$ and kinetic $S^{(e)}$ powers and of the variable component of the electron beam current J along the Cerenkov device at a frequency $\omega/\omega_0 = 0.5$ and electron energies \mathcal{E} of 150 keV (a) and 210 keV (b).

current $I_0 = 1.0$ kA are shown in Fig. 5 a. The last column of Table 3 shows the wavelengths λ of plasma oscillations at various electron energies. As the energy grows, λ increases and may exceed the length of the device.

At an electron energy exceeding the Cerenkov instability threshold, the processes along the device acquire an exponentially increasing (damping) character. The picture of the longitudinal distribution of various quantities for the case of $\mathcal{E} = 210$ keV and $I_0 = 1.4$ kA is shown in Fig. 5 b. One can observe an increase of dragged fields of the electron flow along the device at the expense of lowering of the kinetic energy of the beam.

Thus, the effect of the long-wave Cerenkov instability leads to amplification of electron waves. The coefficient of amplification for the device in question is 10 to 30 db, and this can be used in the construction of new types of microwave devices based on transformation of vortex nonradiated fields of the electron flow into electromagnetic radiated fields.

A similar phenomenon of amplification is also possible in other frequency regions of the long-wave Cerenkov instability that lie above the critical frequency of the decelerating system. In contrast to frequencies lying beyond the bounds, where there are no propagating backward waves, in these regions a feedback and generation of long-wave radiation are possible. This may serve as an explanation of the appearance of the wide-range long-wave component in the spectrum of radiation of experimental devices.

REFERENCES

1. S. I. Bugaev, M. P. Deichuli, V. I. Kanavets, et al., *Radiotekhn. Elektron.*, vol. 32, no. 11, p. 2386, 1987.
2. V. M. Pikunov and I. Yu. Kolesnikova, *Radiotekhn. Elektron.*, vol. 33, no. 11, p. 2381, 1988.
3. I. E. Tamm and I. M. Frank, *Dokl. Akad. Nauk SSSR*, no. 14, p. 107, 1937.
4. L. A. Vainshtein, *Zh. Tekh. Fiz.*, vol. 26, no. 1, p. 126, 1956.
5. V. M. Pikunov and I. A. Chernyavskii, *Radiotekhn. Elektron.*, vol. 37, no. 11, p. 2032, 1992.
6. V. M. Pikunov, V. E. Rodyakin, and A. N. Sandalov, in: *Proceedings of the USSR Seminar. 22-27 May 1991. Part 2. Physics and Application of Microwaves* (in Russian), p. 177, MGU, Moscow, 1991.
7. G. M. Branch and T. G. Mihran, *IRE Trans.*, vol. ED-2, p. 3, 1955.
8. V. M. Pikunov and I. A. Chernyavskii, *Radiotekhn. Elektron.*, vol. 37, no. 11, p. 2041, 1992.
9. W. H. Louisell, *Coupled Mode and Parametric Electronics*, Wiley, New York, London, 1960.